BASE-ISOLATED FCC BUILDING: IMPACT RESPONSE IN NORTHRIDGE EARTHQUAKE

By Satish Nagarajaiah,[1] Member, ASCE, and Xiaohong Sun,[2] Associate Member, ASCE

ABSTRACT: The base-isolated Fire Command and Control (FCC) building in Los Angeles experienced strong motion during the 1994 Northridge earthquake. The California Strong Motion Instrumentation Program has instrumented the building and recorded the data during the Northridge earthquake; these data are available for performance evaluation. Impact was observed in the base-isolated FCC building during the Northridge earthquake. The objective of this study is to evaluate the seismic performance of the base-isolated FCC building during the 1994 Northridge earthquake and the effect of impact. New analytical modeling techniques are developed to analyze the base-isolated FCC building with impact and are verified using system identification. The response computed, using the developed analytical modeling techniques, is verified using recorded data. The response with and without impact is presented. The effects of impact on the structural response are evaluated. The seismic performance evaluations, comparing the response of the base-isolated building with the response if the building were fixed base, are presented. It is shown that the seismic performance of the FCC building in the Northridge earthquake was satisfactory, except for increased shear and drift due to impact. Impact should be avoided in base-isolated structures as it can cause damage.

INTRODUCTION

The Los Angeles County Fire Command and Control (FCC) base-isolated building is a two-story steel frame structure with a high damping elastomeric bearing isolation system. The building is located in the City Terrace area of East Los Angeles, approximately 1 mi southwest of the I-10 and I-710 interchange. The site consists of stiff clay fill underlain by siltstone bedrock (Bachman et al. 1990). The FCC building has been extensively instrumented by the California Strong Motion Instrumentation Program (CSMIP) (Shakal et al. 1994). The elevation, floor plan, and sensor locations are shown in Fig. 1(a). The building experienced strong motion during the 1994 Northridge earthquake. The CSMIP records (Shakal et al. 1994) of the response of the building (CSMIP station No. 24580) during the earthquake provide the data necessary for the evaluation. An examination of the records indicates that impact occurred at the base of the structure, which partially prevented free motion of the base.

The objective of this study is to evaluate the seismic performance of the base-isolated FCC building during the 1994 Northridge earthquake and the effect of impact. This paper presents the developed analytical modeling of the base-isolated FCC building with impact, system identification, response computation and evaluation, and interpretation of structural behavior during the Northridge earthquake. The complete details of this study can be found in Nagarajaiah and Sun (1996, 2000a,b) and Sun (1996).

BASE-ISOLATED FCC BUILDING

The FCC building is a two-story base-isolated building, 57.3 m (188 ft) long and 25.6 m (84 ft) wide, with seven bays in the north-south (NS) direction and three bays in the east-west (EW) direction. Fig. 1(a) shows the plan and elevation of the building. The superstructure is a braced frame consisting of 32 steel wide flange columns, which are in turn supported by 32 high damping rubber bearings. The superstructure chevron bracing is located at the building perimeter. The base, first floor, and roof are made up of concrete slabs on metal decking. The metal decking is supported on a grid of steel beams. The base level steel beam framing system is moment connected to the columns to resist moments transferred from the isolators.

Elastomeric Isolation System

The isolation system is made up of 32 high damping rubber bearings. The bearings are 40.64 cm (16 in.) square with a height of 36.07 cm (14.2 in.); bearings are made up of 27 layers of rubber with 0.95-cm (0.373-in.) thickness and 26 layers of steel shims of 0.19-cm (0.0747-in.) thickness. The steel end plates are 2.54 cm (1 in.) thick and bolted to the column and the foundation. The bearings at the building perimeter have an 11.68-cm (4.6-in.) diameter hole, which houses the ultimate restraint device (Seible and Priestley 1989); the ultimate restrainers engage at 31.75 cm (12.5 in.).

Recorded Response in Northridge Earthquake

The building has been instrumented by CSMIP (Shakal et al. 1994); the sensor locations are shown in Fig. 1(a). The sensors (accelerometers) are located at the foundation, first floor, second floor, and roof in the NS and EW directions. The peak values of the recorded acceleration, in the EW and NS directions, during the Northridge earthquake are shown in Table 1. The acceleration time histories and the acceleration response spectra are presented in Fig. 2. The foundation/ground acceleration, CHN5–CHN7, presented in Fig. 2(a) and the corresponding spectra presented in Fig. 2(b) indicate that the spectral accelerations were larger in the EW direction than the NS direction.

The acceleration time histories of CHN9–CHN11 at the base level and of CHN14–CHN16 at the roof level in the EW direction, shown in Figs. 2(c and e), exhibit sharply increased higher mode response, in each upper half-cycle, between the 12- and 16-s time interval, increasing the acceleration from $0.22g$ at the foundation level to $0.32g$ at the roof level. The increased higher mode response was caused by one-sided impact against the concrete entry bridge [Fig. 1(c)] in the northeast corner of the building—reported in the reconnaissance report by the Earthquake Engineering Research Institute (EERI), El Cerrito, Calif. (1996)—which is evident from the analysis results to be presented in the following sections. The impact caused the higher acceleration of $0.35g$ in CHN11, which is the sensor close to the northeast corner of the build-

[1]Assoc. Prof., Dept. of Civ. Engrg., Rice Univ., Houston, TX 77005. E-mail: nagaraja@rice.edu

[2]Des. Engr., CBM Engineers, Houston, TX 77004.

Note. Associate Editor: Brad Cross. Discussion open until February 1, 2002. To extend the closing date one month, a written request must be filed with the ASCE Manager of Journals. The manuscript for this paper was submitted for review and possible publication on August 8, 2000; revised March 16, 2001. This paper is part of the ***Journal of Structural Engineering***, Vol. 127, No. 9, September, 2001. ©ASCE, ISSN 0733-9445/01/0009-1063–1075/$8.00 + $.50 per page. Paper No. 22502.

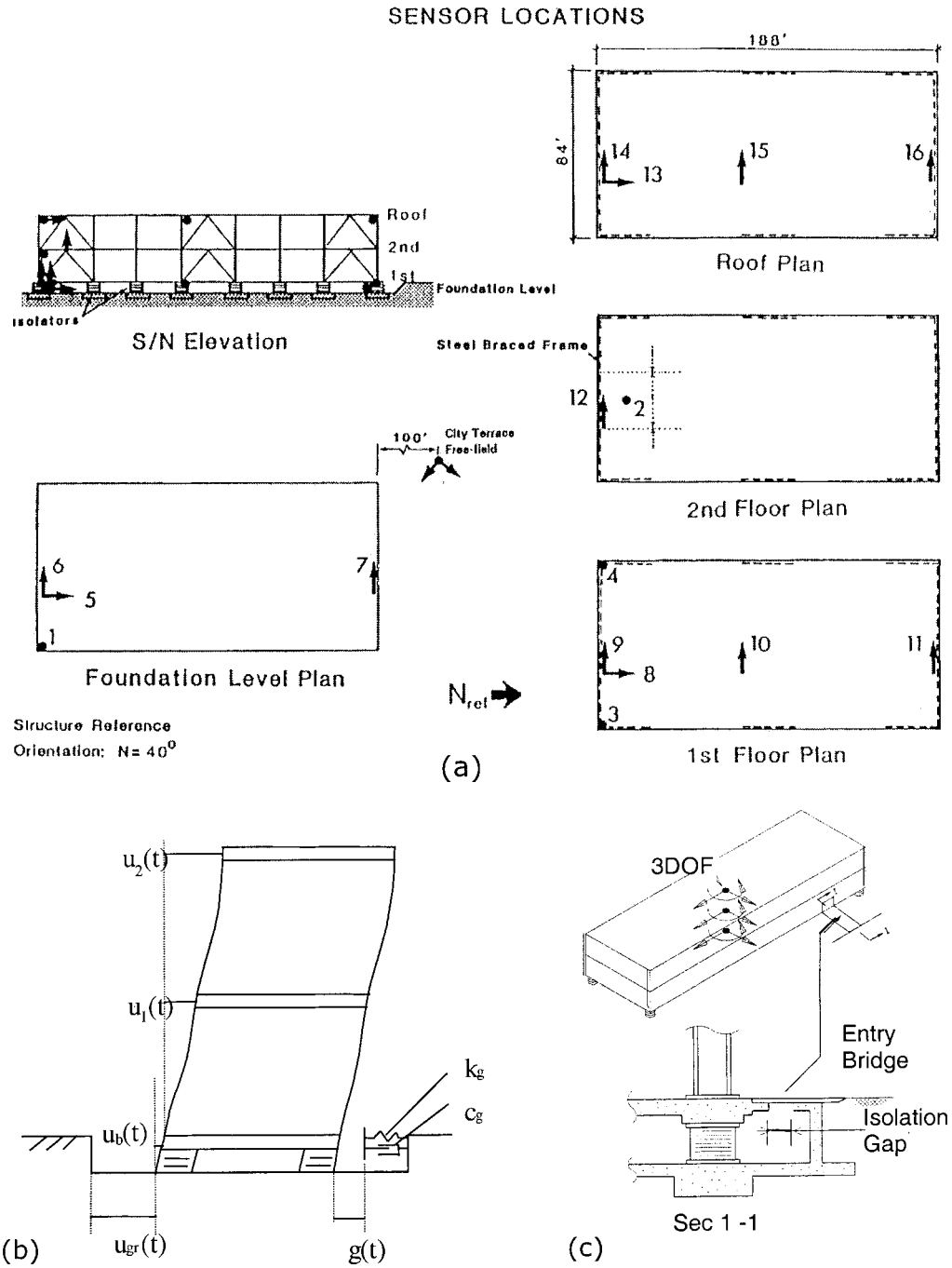

FIG. 1. FCC Building: (a) Elevation, Plan, and Sensor Locations; (b) Analytical Model; (c) Entry Bridge and Isolation Gap

TABLE 1. Recorded Peak Values of Response in EW and NS Directions [See Fig. 1(a) for Sensor Locations]

Channel number	Acceleration *g*
6	0.22
7	0.19
9	0.21
10	0.23
11	0.35
14	0.24
15	0.32
16	0.25
5	0.18
8	0.07
13	0.09
Free field	0.32

ing. The entry bridge was designed to allow free motion during an earthquake; however, it was constructed incorrectly, preventing free motion until such time that it gave way.

In the NS direction base isolation deamplified the acceleration from 0.18*g* in CHN5 at the foundation level to 0.09*g* in CHN13 at the roof level, as shown in Fig. 3(a). The spectral accelerations of the base and roof are shown in Fig. 3(b). There is no evidence of impact in the NS direction from the time histories shown in Fig. 3.

ANALYTICAL MODELING OF BASE-ISOLATED FCC BUILDING WITH IMPACT

The analysis is accomplished in two phases. The first phase involves development of a 2D analytical model. The 2D analysis is essential to estimate the dynamic properties effective

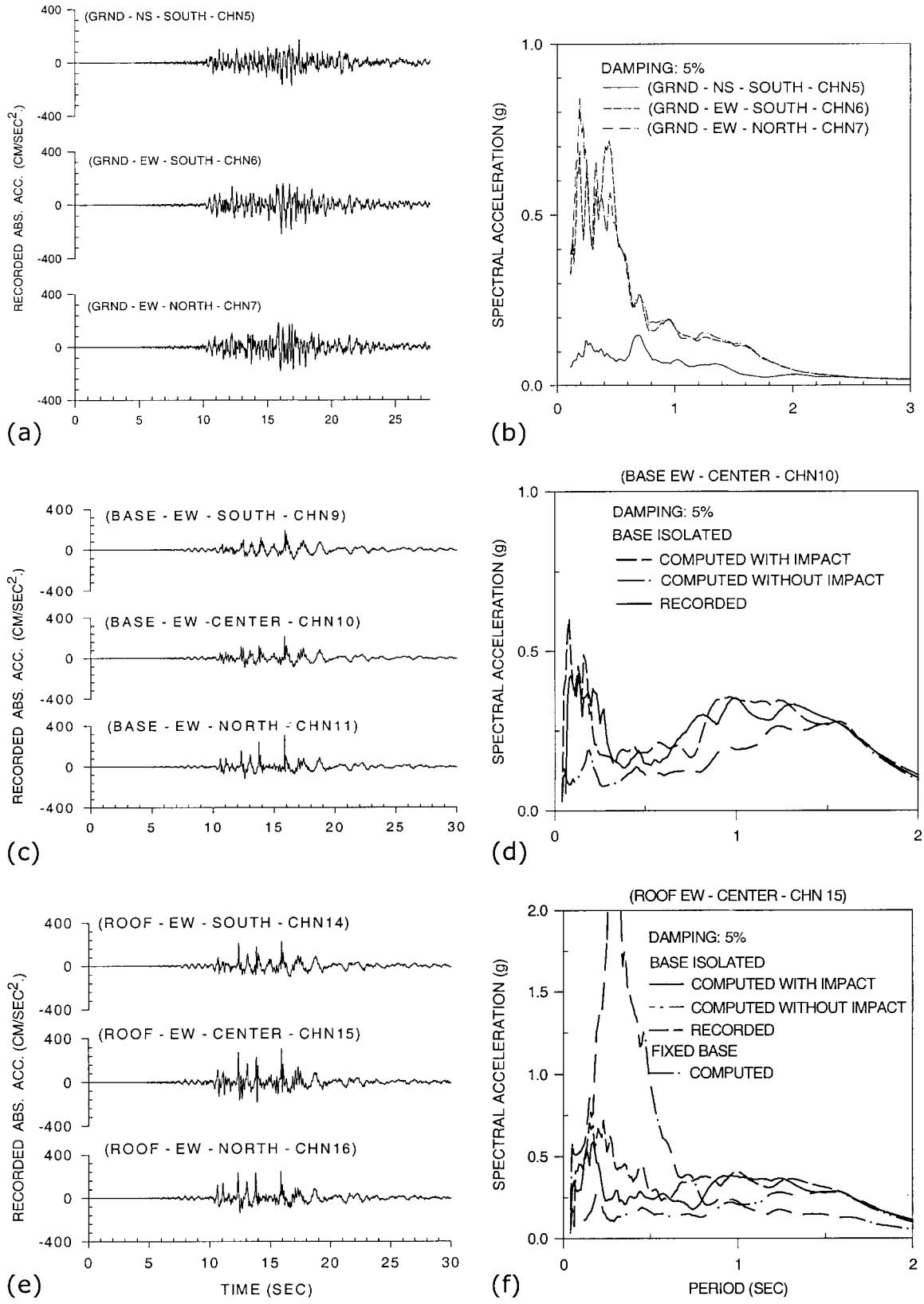

FIG. 2. In NS and EW Direction (See Fig. 1 for Sensor Locations): (a), (c), (e) Recorded Acceleration Time History; (b), (d), (f) Response Spectra

during impact, such as the impact-spring-dashpot parameters, and to compute the lateral response. The second phase is to perform 3D analysis to account for eccentric impact, with respect to the center of mass, and to compute the lateral-torsional response. Both 2D and 3D analytical modeling techniques are developed in this study (Nagarajaiah and Sun 1995, 1996; Sun 1996).

2D DYNAMICS ANALYSIS

The developed 2D analytical model with one-sided impact (Maison and Kasai 1990) consists of a linear system before and after impact and a different linear system during impact (Nagarajaiah and Sun 1996; Sun 1996). The superstructure is modeled as a linear multi-degree of freedom system. The elas-

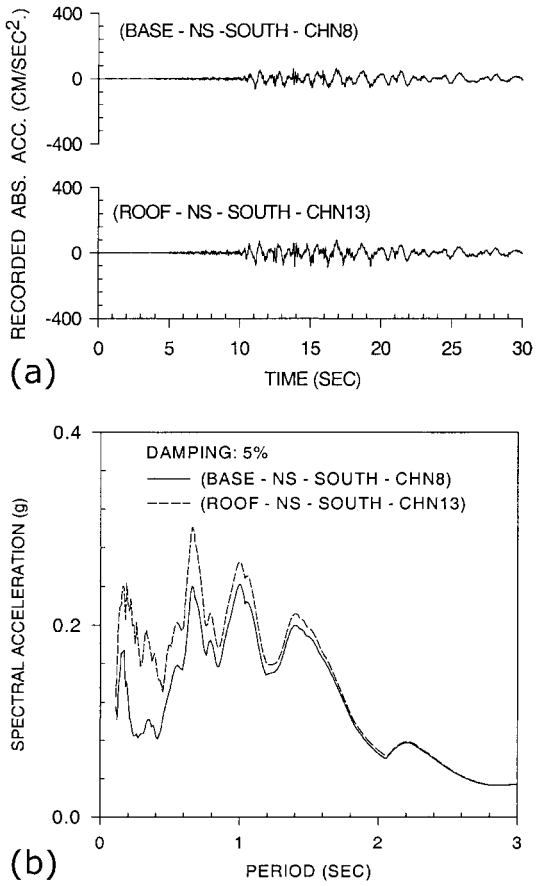

FIG. 3. In NS Direction (See Fig. 1 for Sensor Locations): (a) Recorded Acceleration Time Histories: (b) Response Spectra

tomeric isolation system is modeled using equivalent linear stiffness and damping; the nonlinearities of the elastomeric bearings are not considered. The entry bridge is represented by a linear impact spring and dashpot. Hence, the combined system, consisting of the superstructure and isolation system, is completely linear during (1) State 1—when the structure is free to vibrate, without any contact with the impact element, prior to and after impact; and (2) State 2—when the structure is in contact with the impact element, during impact. The changes in stiffness from State 1 to State 2 and vice versa results in nonlinear response. The time varying gap between the base slab and the entry bridge is considered in the dynamic analysis. The complete formulation (Nagarajaiah and Sun 1996; Sun 1996) with appropriate conditions for state change is as follows.

State 1

In State 1 the structure is free to vibrate without any contact with the impact-spring-dashpot system, as shown in Fig. 1(b). The equations of motion of the system in State 1 are

$$\mathbf{M}^*\ddot{\mathbf{u}}^*(t) + \mathbf{C}^*\dot{\mathbf{u}}^*(t) + \mathbf{K}^*\mathbf{u}^*(t) = -\mathbf{M}^*\mathbf{R}^*\ddot{\mathbf{u}}_{gr}(t) \quad (1)$$

where $\mathbf{u}^* = [u_n^*, \ldots, u_i^*, \ldots, u_1^*, u_b]$ = vector of floor and base displacements, with respect to the ground, where $u_i^* = u_i + u_b$, u_i = floor displacement with respect to the base, u_b = base displacement with respect to the ground, and u_{gr} = ground displacement, as shown in Fig. 1(b); $\mathbf{M}^*$, $\mathbf{C}^*$, and $\mathbf{K}^*$ = mass, damping, and linear stiffness matrices of the combined system consisting of the superstructure and the isolation system; and $\mathbf{R}^*$ = influence matrix. The damping in the isolation system is typically larger than that of the superstructure. The damping matrix $\mathbf{C}^*$ is not proportional to stiffness $\mathbf{K}^*$ or the mass matrix $\mathbf{M}^*$. Thus, complex eigenvalue analysis is necessary. The damping matrix does not become diagonal (or uncoupled), under modal transformation if undamped mode shapes are used; hence, off-diagonal coupling terms exist. However, for the nonproportional damping ratio of 16% in the isolation system, considered in this study, the equations can be uncoupled and the off-diagonal terms neglected (Kelly 1993) with normal modal transformation using the State 1 undamped modal property. Using normal mode coordinates

$$\mathbf{u}^*(t) = \boldsymbol{\phi}^*\mathbf{y}(t) \quad (2)$$

in which $\boldsymbol{\phi}^*$ = modal matrix of the linear base-isolated structure, normalized with respect to the mass matrix; and $\mathbf{y}(t)$ = modal displacement vector. The resulting uncoupled equations are

$$\ddot{y}_j(t) + 2\xi_j^*\omega_j^*\dot{y}_j(t) + \omega_j^{*2}y_j(t) = -p_j^*\ddot{u}_{gr}(t) \quad (3)$$

in which, $y_j(t)$, $\dot{y}_j(t)$, and $\ddot{y}_j(t)$ = jth model displacement, velocity, and acceleration at time t, respectively; ω_j^* = jth modal frequency; ξ_j^* = jth mode damping ratio; $p_j^* = \varphi_j^{*T}\mathbf{M}^*\mathbf{R}^*$, the jth modal participation factor; and $\boldsymbol{\phi}_j^*$ = jth modal vector.

State 2

The building is in contact with the impact-spring-dashpot element. The equations of motion are

$$\mathbf{M}^*\ddot{\mathbf{u}}^*(t) + \mathbf{C}^*\dot{\mathbf{u}}^*(t) + \mathbf{K}^*\mathbf{u}^*(t) + \mathbf{f}^*(t) = -\mathbf{M}^*\mathbf{R}^*\ddot{\mathbf{u}}_{gr}(t) \quad (4)$$

where $\mathbf{f}^*(t) = \mathbf{r}k_g\mathbf{u}_b(t) - \mathbf{r}k_g\mathbf{g}(t) + \mathbf{r}c_g\dot{\mathbf{u}}_b(t)$ = impact force; the impact-spring-dashpot element consists of spring $\mathbf{k}_g$ and dashpot $\mathbf{c}_g$; $\mathbf{r}^T = [0\ 0\ 0\ \cdots\ 0\ 1]$; and $\mathbf{g}(t)$ = time dependent gap. Rearranging (4)

$$\mathbf{M}^*\ddot{\mathbf{u}}^*(t) + \mathbf{C}^*\dot{\mathbf{u}}^*(t) + \mathbf{K}^*\mathbf{u}^*(t) + \mathbf{r}k_g\mathbf{u}_b(t) + \mathbf{r}c_g\dot{\mathbf{u}}_b(t) = -\mathbf{M}^*\mathbf{R}^*\ddot{\mathbf{u}}_{gr}(t) + \mathbf{r}k_g\mathbf{g}(t) \quad (5)$$

$$\mathbf{M}^*\ddot{\mathbf{u}}^*(t) + \bar{\mathbf{C}}^*\dot{\mathbf{u}}^*(t) + \bar{\mathbf{K}}^*\mathbf{u}^*(t) = -\mathbf{M}^*\mathbf{R}^*\ddot{\mathbf{u}}_{gr}(t) + \mathbf{r}k_g\mathbf{g}(t) \quad (6)$$

where $\bar{\mathbf{K}}$ and $\bar{\mathbf{C}}$ = stiffness and damping matrices in State 2, including the term with $\mathbf{k}_g$ and $\mathbf{c}_g$. The term $\mathbf{r}k_g\mathbf{g}(t)$ is treated as a pseudoforce term. The force in the impact element

$$\mathbf{f}^*(t) = \mathbf{r}k_g(\mathbf{u}_b(t) - \mathbf{g}(t)) + \mathbf{r}c_g\dot{\mathbf{u}}_b(t) \quad \text{if } \mathbf{u}_b(t) \geq \mathbf{g}(t), \text{ State 2} \quad (7a)$$

$$\mathbf{f}^*(t) = 0 \quad \text{if } \mathbf{u}_b(t) < \mathbf{g}(t), \text{ State 1} \quad (7b)$$

The impact element can only resist compressive forces. Equations of motion in State 2 given by (6) can be uncoupled (neglecting the coupling due to nonproportional or nonclassical damping) by transformation to normal mode coordinates using State 2 undamped modal properties. The resulting uncoupled equations are

$$\ddot{y}_j(t) + 2\xi_j^*\omega_j^*\dot{y}_j(t) + \omega_j^{*2}y_j(t) = -p_j^*\ddot{u}_{gr}(t) + \bar{p}_j^*k_g g(t) \quad (8)$$

where $p_j^*k_g g(t)$ = jth modal pseudoforce associated with the impact element; $\bar{p}_j^* = \varphi_j^{*T}r$; and ω_j^*, ξ_j^*, and φ_j^* = properties in State 2.

Solution Procedure

The uncoupled equations of motion can be solved explicitly using a piecewise exact method (Nigam and Jennings 1969). The method is based on the exact solution of the equations of motion of a structure subjected to loading that varies linearly during a discrete time interval. Assuming ground acceleration varies linearly during each step

$$\ddot{u}_{gr}(t_{i+1}) = \ddot{u}_{gr}(t_i) + \alpha\Delta t \quad (9)$$

where $\ddot{u}_{gr}(t_i)$ and $\ddot{u}_{gr}(t_{i+1})$ = ground acceleration at times t_i and t_{i+1}, respectively; Δt = time step $\Delta t = (t_{i+1} - t_i)$; and α = rate of change of the ground acceleration during the time step.

State 1

The solutions for the displacement, velocity, and acceleration in State 1 at t_{i+1} are as follows:

$$y_j(t_{i+1}) = A_0 + A_1\Delta t + A_2 e^{-\xi_j\omega_j\Delta t}\cos(\omega_{dj}\Delta t) + A_3 e^{-\xi_j\omega_j\Delta t}\sin(\omega_{dj}\Delta t) \quad (10)$$

$$\dot{y}_j(t_{i+1}) = A_1 + (A_3\omega_{dj} - A_2\xi_j\omega_j)e^{-\xi_j\omega_j\Delta t}\cos(\omega_{dj}\Delta t) - (A_2\omega_{dj} + A_3\xi_j\omega_j)e^{-\xi_j\omega_j\Delta t}\sin(\omega_{dj}\Delta t) \quad (11)$$

$$\ddot{y}_j(t_{i+1}) = (A_2\omega_{dj} + A_3\xi_j\omega_j)e^{-\xi_j\omega_j\Delta t}(\xi_j\omega_j\sin(\omega_{dj}\Delta t) - \omega_{dj}\cos(\omega_{dj}\Delta t)) - (A_3\omega_{dj} - A_2\xi_j\omega_j)e^{-\xi_j\omega_j\Delta t}(\xi_j\omega_j\cos(\omega_{dj}\Delta t) + \omega_{dj}\sin(\omega_{dj}\Delta t)) \quad (12)$$

where

$$A_0 = \frac{\bar{f}(t_i)}{\omega_j^2} + \frac{2\xi_j p_j\alpha}{\omega_j^3};\quad \bar{f}(t_i) = -p_j\ddot{u}_{gr}(t_i);\quad A_1 = -\frac{p_j\alpha}{\omega_j^2}$$

$$A_2 = y_j(t_i) - A_0;\quad A_3 = \frac{1}{\omega_{dj}}\left(\dot{y}_j(t_i) + A_2\xi_j\omega_j + \frac{p_j\alpha}{\omega_j^2}\right)$$

$$\omega_{dj} = (\omega_j\sqrt{1-\xi_j^2})$$

equal the jth modal damped frequency.

The displacement, velocity, and acceleration responses for State 1 can be obtained from (2). The properties in State 1 are used for the solution procedure until state change is detected based on the conditions to be described next.

State 2

For State 2, the same set of equations [(10)–(12)] are applicable with State 2 frequencies and damping ratios, and $f(t_i) = -p_j^*\ddot{u}_{gr}(t_i) + \bar{p}_j^* k_g g(t_i)$. The properties in State 2 are used for the solution procedure until state change is detected based on the conditions to be described next.

Conditions for State Change

In the solution procedure, the final displacement and velocity of one state become the initial conditions for the next state. The base displacement, velocity, and acceleration responses in States 1 or 2 are computed from (1)–(12) at time t_{i+1}. When the base displacement $u_b(t_{i+1})$ equals the gap size $g(t)$, a state change will occur according to the following rules:

- When $u_b(t_{i+1})$ equals $g(t)$ and $\dot{u}_b(t_{i+1})$ is negative, the response is in State 1 and (1) for State 1 applies with appropriate initial conditions.
- When $u_b(t_{i+1})$ equals $g(t)$ and $\dot{u}_b(t_{i+1})$ is positive, the response is in State 2 and (6) for State 2 applies with appropriate initial conditions.

Also, the impact element can only resist compressive forces.

3D DYNAMIC ANALYSIS

The superstructure and the base are modeled linearly with 3 master degrees of freedom (DOF) per floor at the center of mass. The base and floors are assumed to be infinitely rigid in plane. The equations of motion for the superstructure are

$$\mathbf{M}\ddot{\mathbf{u}} + \mathbf{C}\dot{\mathbf{u}} + \mathbf{K}\mathbf{u} = -\mathbf{M}\mathbf{R}(\ddot{\mathbf{u}}_{gr} + \ddot{\mathbf{u}}_b) \quad (13)$$

where $\mathbf{M}$, $\mathbf{C}$, and $\mathbf{K}$ = superstructure mass, damping, and linear stiffness matrices in the fixed base condition, respectively; $\mathbf{R}$ = influence matrix; $\mathbf{u}$ = floor displacement vector, relative to the base; $\mathbf{u}_b$ = vector of base displacement relative to the ground; and $\ddot{\mathbf{u}}_{gr}$ = vector of ground acceleration [Figs. 1(b and c)].

The equations of motion for the base are

$$\mathbf{R}^T\mathbf{M}[\ddot{\mathbf{u}} + \mathbf{R}(\ddot{\mathbf{u}}_b + \ddot{\mathbf{u}}_{gr})] + \mathbf{M}_b(\ddot{\mathbf{u}}_b + \ddot{\mathbf{u}}_{gr}) + \mathbf{C}_b\dot{\mathbf{u}}_b + \mathbf{K}_b\mathbf{u}_b + \mathbf{f} = 0 \quad (14)$$

in which $\mathbf{M}_b$ = diagonal mass matrix of the rigid base; $\mathbf{C}_b$ = resultant damping matrix of equivalent viscous damping in the bearings; $\mathbf{K}_b$ = resultant equivalent linear stiffness matrix of isolation bearings; and $\mathbf{f}$ = forces in the impact element [$\mathbf{f}^*(t)$ in (7)] transformed to the center of mass of the base using the rigid base slab assumption. Employing modal reduction

$$\mathbf{u} = \boldsymbol{\phi}\mathbf{u}^0 \quad (15)$$

in which $\boldsymbol{\phi}$ = modal matrix of the fixed-base superstructure, normalized with respect to the mass matrix; and $\mathbf{u}^0$ = modal displacement vector relative to the base. Combining (13)–(15), the following matrix equation is obtained:

$$\begin{bmatrix}\boldsymbol{\phi}^T\mathbf{M}\boldsymbol{\phi} & \boldsymbol{\phi}^T\mathbf{M}\mathbf{R}\\ \mathbf{R}^T\mathbf{M}\boldsymbol{\phi} & \mathbf{R}^T\mathbf{M}\mathbf{R} + \mathbf{M}_b\end{bmatrix}\begin{Bmatrix}\ddot{\mathbf{u}}^0\\ \ddot{\mathbf{u}}_b\end{Bmatrix} + \begin{bmatrix}\boldsymbol{\phi}^T\mathbf{C}\boldsymbol{\phi} & \mathbf{O}\\ \mathbf{O} & \mathbf{C}_b\end{bmatrix}\begin{Bmatrix}\dot{\mathbf{u}}^0\\ \dot{\mathbf{u}}_b\end{Bmatrix} + \begin{bmatrix}\boldsymbol{\phi}^T\mathbf{K}\boldsymbol{\phi} & \mathbf{O}\\ \mathbf{O} & \mathbf{K}_b\end{bmatrix}\begin{Bmatrix}\mathbf{u}^0\\ \mathbf{u}_b\end{Bmatrix} + \begin{Bmatrix}\mathbf{O}\\ \mathbf{f}\end{Bmatrix} = -\begin{bmatrix}\boldsymbol{\phi}^T\mathbf{M}\mathbf{R}\\ \mathbf{R}^T\mathbf{M}\mathbf{R} + \mathbf{M}_b\end{bmatrix}\ddot{\mathbf{u}}_{gr} \quad (16)$$

Because the modal matrix $\boldsymbol{\phi}$ is normalized with respect to mass, the following diagonal matrices are obtained $\boldsymbol{\phi}^T\mathbf{M}\boldsymbol{\phi} = \mathbf{I}$, $\boldsymbol{\phi}^T\mathbf{K}\boldsymbol{\phi} = \boldsymbol{\omega}^2$, and $\boldsymbol{\phi}^T\mathbf{C}\boldsymbol{\phi} = 2\boldsymbol{\zeta}\boldsymbol{\omega}$, where $\boldsymbol{\omega}$ = diagonal matrix of natural frequencies of the fixed-base structure and $\boldsymbol{\zeta}$ = diagonal matrix of damping ratios of the fixed-base structure. Note that (16) accounts for the nonproportional damping due to the term $\mathbf{C}_b$.

Eq. (16) is solved using an efficient semi-implicit pseudoforce solution algorithm (Nagarajaiah et al. 1991a,b). In the pseudoforce method, the forces $\mathbf{f}$ in (16) are moved to the right-hand side of the equations of motion and solved by iteration until convergence is reached. Note that the left-hand side of (16) is completely linear in this approach; $\mathbf{f}$ and the conditions of state change are represented by the pseudoforce term on the right-hand side. Numerically this approach is stable because of the semi-implicit iterative procedure used. The formulation in (16) with impact is implemented in the computer program 3D-BASIS (Nagarajaiah et al. 1991a,b).

2D and 3D SUPERSTRUCTURE AND ISOLATION SYSTEM MODELING

Superstructure and isolation system modeling is performed in both 3D and 2D. The linear 2D model of the superstructure is obtained by condensing the linear 3D model. A detailed 3D

TABLE 2. Computed and Identified Periods of Fixed-Base Building (3D)

MODE (1)	Computed T-sec EW (2)	Computed T-sec NS (3)	Computed T-sec Torsion (4)	Identified T-sec (Hz) EW (5)
1	0.37	0.32	0.19	0.35 (2.86)
2	0.13	0.12	0.08	0.11 (8.9)

model of the superstructure in the fixed-base condition is developed with a rigid floor slab assumption. The building properties—such as beam, column, bracing, and floor slab details—used for analytical modeling are computed from building drawings provided by CSMIP. Three master DOF at the center of mass of each floor are used in the condensed model, as shown in Fig. 1(c); hence, only 6 DOF (2 floors × 3 master DOF/floor) are retained for modeling the FCC building in the fixed-base condition. The six periods in the fixed-base condition are shown in Table 2 (columns 2–4). A damping ratio of 5% is assumed for all six modes. A combined analytical model of the superstructure and the isolation system is developed using (16) with 9 master DOF. The superstructure is modeled using 6 master DOF and 6 modes in the fixed-base condition, and the isolation system is modeled using 3 master DOF and equivalent linear stiffness and damping properties. The isolation system properties are extracted from prototype test results (Seible and Priestley 1989). The equivalent linear stiffness of each elastomeric bearing at 3.5 cm (1.4 in.)—maximum displacement experienced by the isolators in the Northridge earthquake—is 12.25 kN/cm (7 kip/in.) and estimated damping is 16%. The periods of the 3D base-isolated structure with an equivalent linear isolation system are shown in Table 3 (columns 2–4).

A 2D model is formulated using the 2D version of (16) with fixed-base properties in the EW direction ($T_{1,2}$ = 0.37 and 0.13

TABLE 3. Computed and Identified Periods and Damping Ratios of Base-Isolated FCC Building (3D/2D)

	3D Computed T (s)			2D Computed		Identified T	Identified	
				T^* (s)	ξ^* (%)	[s (Hz)]	T^* (s)	ξ^* (%)
Mode	EW	NS	Torsion	EW	EW	EW	EW	EW
(1)	(2)	(3)	(4)	(5)	(6)	(7)	(8)	(9)
1	1.37	1.36	1.17	1.38	0.14	1.25 (0.8)	1.34	0.11
2	0.24	0.20	0.12	0.21	0.12	0.21 (4.76)	0.18	0.1
3	0.12	0.11	0.07	0.12	0.05	—	0.11	0.05

TABLE 4. Computed and Identified Periods and Damping Ratios of Base-Isolated FCC Building (2D)

MODE	Computed					Identified	Identified	
	State 1 EW		State2 EW		Combined State 1+2 EW	Combined State 1 + 2 EW	Combined State 1+2 EW	
(1)	T^* - sec (2)	ξ^* - % (3)	T^* - sec (4)	ξ^* - % (5)	T – sec (6)	T-sec(Hz) (7)	T – sec (8)	ξ - % (9)
1	1.38	0.14	0.43	0.03	0.88	0.84 (1.2)	0.94	0.08
2	0.21	0.12	0.16	0.09	0.18	-	0.18	0.1
3	0.12	0.05	0.10	0.06	0.1	-	0.11	0.05

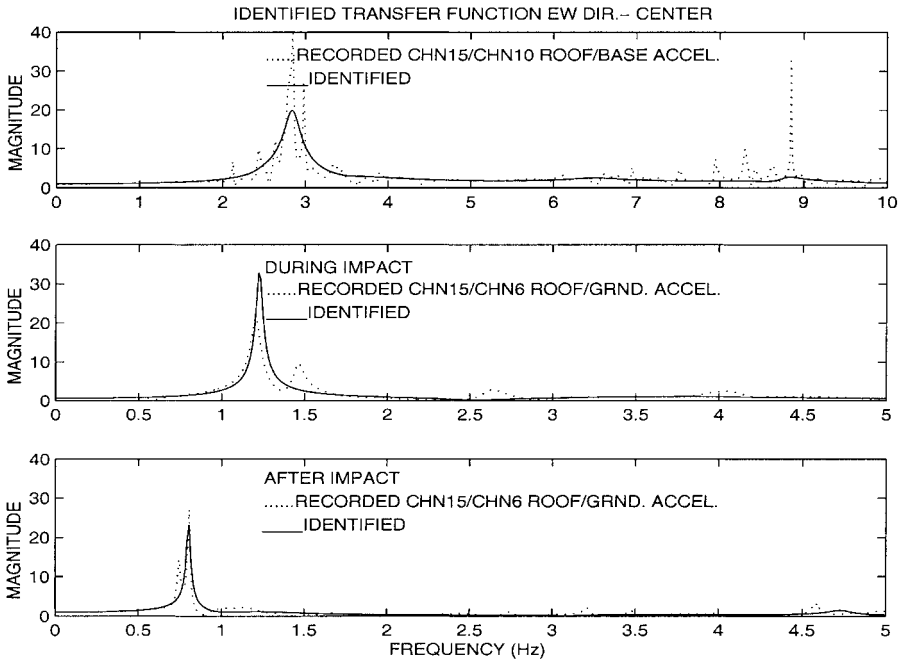

FIG. 4. Recorded and Identified Transfer Functions in EW Direction: (a) Fixed Base; (b) Base Isolated with Impact; (c) Base Isolated without Impact

s and $\zeta_{1,2}$ = 5%) and isolation properties (K_b = 12.25 kN/cm and ξ_b = 16%). This approach is necessary to estimate the damping ratios in State 1 and to estimate the damping matrix **C***. Complex eigenvalue analysis is performed and the results are presented in Table 3 (columns 5 and 6).

System properties for 2D analysis are calculated separately for States 1 and 2. Both classical eigenvalue analysis and nonclassical complex eigenvalue analysis are performed. The computed frequencies and damping ratios, based on complex eigenvalue analysis and (1), for State 1 (prior to and after impact, no contact with impact spring) are shown in Table 4 (columns 2 and 3)—the values are the same as in Table 3 (columns 5 and 6). Note that in (3) classical eigenvalue analysis results—the frequencies being nearly the same and damping ratios as shown in Table 4—are used. To calculate the State 2 (during impact) properties, the impact spring property needed is evaluated next.

SYSTEM IDENTIFICATION

Despite the nonlinear response of the FCC building, because of changes in stiffness from State 1 to State 2 and vice versa, useful estimates of the equivalent linear structural properties can be obtained by using system identification techniques. The actual dynamic characteristics of the building, existing during the Northridge earthquake, are estimated based on the identified and recorded transfer functions obtained from the recorded input and output responses (Nagarajaiah and Sun

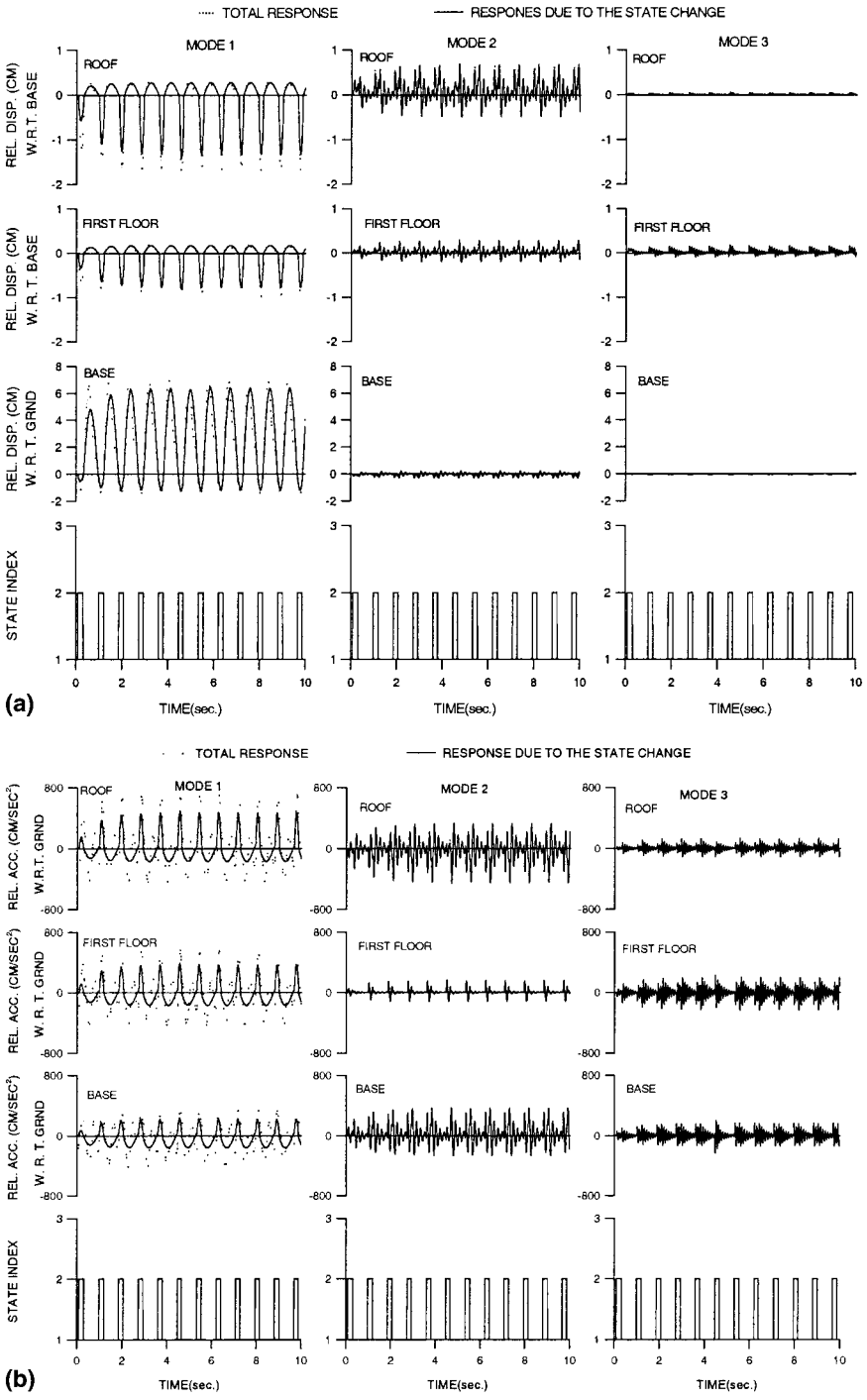

FIG. 5. Harmonic 2D Response with One-Sided Impact: (a) Displacement Response Time Histories; (b) Acceleration Response Time Histories; (c) Frequency Response Curves (Relative Displacement Normalized with Respect to Bearing Height)

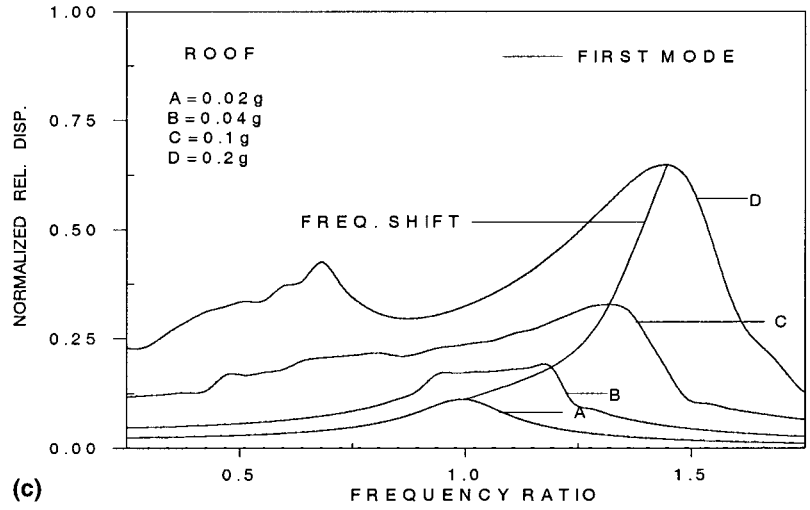

FIG. 5. (*Continued*)

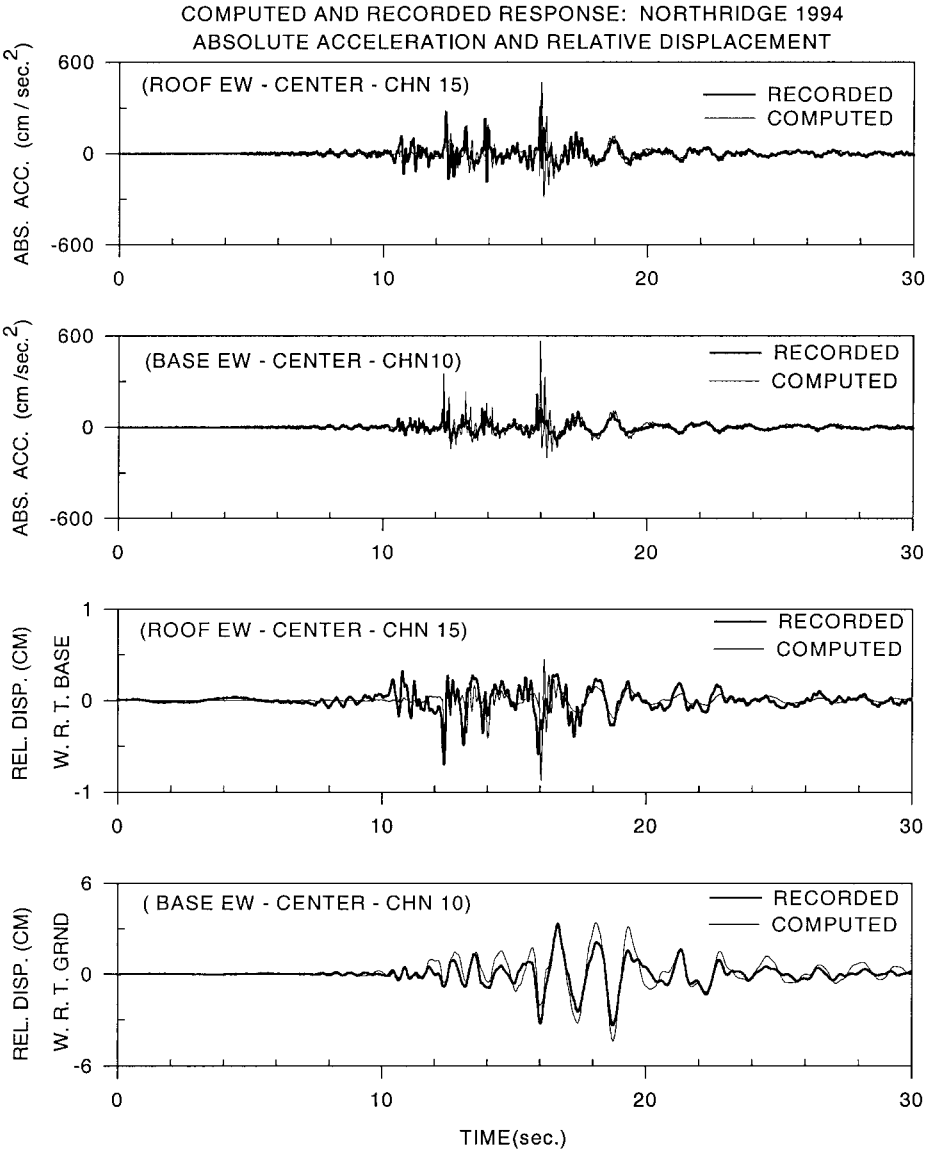

FIG. 6. Comparison of Recorded and Computed 2D Response with Impact in EW Direction

2000a,b). Parametric identification methods (Ljung 1987) are used to obtain periods and damping ratios from the transfer functions obtained using nonparametric methods (Ljung 1987) and recorded input and output responses. The analytical model is verified by comparing the computed and identified periods/damping ratios.

Parametric Identification

The system transfer function $H(z)$ relating input and output (Nagarajaiah and Sun 2000a,b) is

$$H(z) = \frac{Y(z)}{X(z)} = \frac{\sum_{k=0}^{nb} b(k)z^{-k}}{\sum_{k=0}^{na} a(k)z^{-k}} \tag{17}$$

where $z = e^{(\sigma \pm i w)\Delta T}$, and a, b = constants. The roots of the denominator polynomial are the poles of $H(z)$. The roots of the numerator polynomial are zeros of $H(z)$. For a stable system, all poles must have magnitude <1 and should be located within the unit circle. The jth pole of $H(z)$ is given by

$$z_j = \exp[(-\xi_j \omega_j \pm i\omega_j \sqrt{1 - \xi_j^2})\Delta T] \tag{18}$$

where ΔT = sampling interval; and ω_j and ξ_j = frequency and damping ratio of the jth mode of vibration. The frequency and damping ratio can be determined as follows:

$$\omega_j = \frac{1}{\Delta T}\sqrt{\ln^2 r_j + \theta_j^2}; \quad \xi_j = -\frac{\ln r_j}{\sqrt{\ln^2 r_j + \theta_j^2}} \tag{19}$$

where $r_j = |z_j|$, the magnitude; and $\xi_j = \tan^{-1}[\mathrm{Im}(z_j)/\mathrm{Re}(z_j)]$, the phase angle of the jth pole. The poles are in complex conjugate pairs; hence, the number of identifiable modes is equal to $na/2$.

Nonparametric Identification

The power spectral density (PSD) P_{xx} obtained from z transform of autocorrelation is related to the cross-spectral density (CSD) P_{xy} obtained from z transform of cross correlation as follows (Ljung 1987):

$$P_{xy}(z) = H(z^{-1})P_{xx}(z) \tag{20}$$

which can also be written as a function of $\boldsymbol{\omega}$

$$P_{xy}(\omega) = H(\omega)P_{xx}(\omega) \tag{21}$$

The acceleration transfer function estimate is obtained using PSD and CSD. Hanning window is applied to sections and modified periodograms are computed. An average of four modified periodograms are adopted for computing PSD and CSD and for estimating transfer functions. Additional averaging would reduce the variance of the estimate; however, four averages are found to be sufficiently accurate. An overlap length of half the section length is used to reduce the variance of the estimate. Parametric modeling is performed using (17) with $na = 22$ and $nb = 20$. The evaluation of the parameters is based on the minimization of the weighted sum of squares of errors between the absolute magnitudes of the actual and desired frequency response function points.

The poles, frequencies, and damping ratios are obtained from the identified transfer functions. The recorded and identified transfer functions are presented in Fig. 4.

Fixed-Base Case

As per (13)–(16), the frequencies and damping ratios of the structure, if it were to be fixed base, can be estimated by means of the roof/base transfer function. In Fig. 4(a) the recorded and identified transfer function of the fixed-base case (CHN15-roof/CHN10-base) is shown. The identified periods in the EW direction for the fixed-base case are shown in Table 2. The damping values in the fixed-base case could not be identified reliably; hence, they are not shown. The comparison between the computed and identified periods indicate good agreement.

Base-Isolated Case with Impact

Impact occurred between 12 and 16 s. The recorded and identified transfer function of the base-isolated case with impact obtained from roof/ground acceleration, between 12 and 16 s, is shown in Fig. 4(b). The identified first mode frequency of 1.2 Hz or period of 0.84 s, in the EW direction, is shown in Table 4 (column 7)—which represents the equivalent linear frequency of the nonlinear system involving a combination of State 1 (prior to and after impact, no contact with impact spring) and State 2 (during impact). The second and third mode frequencies are not shown in Table 4, as they could not be reliably identified. Nagarajaiah (2001) has obtained the frequencies and damping ratios of all three modes by using time domain system identification techniques; the results are shown in Table 4 (columns 8 and 9). The computed first mode period is 0.88 s, as shown in Table 4 (column 6); also shown are the second and the third mode periods. The details of how the computed periods were obtained will be discussed in the next section. The comparison between the computed and identified periods is satisfactory. Note that both periods and damping ratios in the nonlinear combined state are nearly the averages of State 1 and State 2 properties.

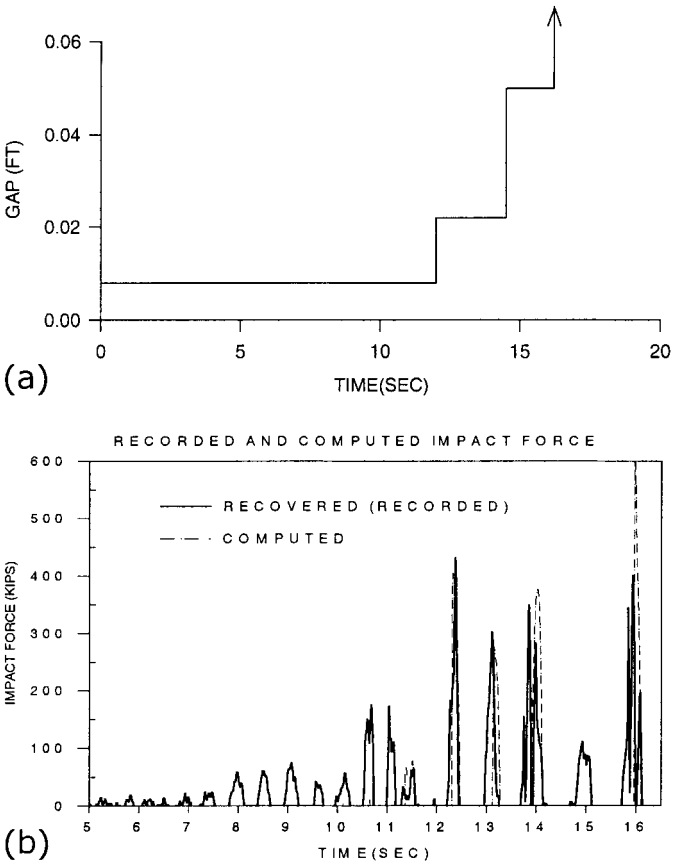

FIG. 7. 2D Dynamic Response: (a) Estimated Gap Time History at Entry Bridge (Note That Gap Opens Completely after 16.2 s); (b) Comparison between Recovered and Computed Impact Force Time History

Base-Isolated Case

In Fig. 4(c) the recorded and identified transfer function of the base-isolated structure, after the impact ceased and base isolation was fully effective (State 1), is shown. The computed and identified periods in the EW direction of the base-isolated FCC building (State 1) are shown in Table 3 (columns 5–7) and Table 4 (columns 2 and 3). The third mode frequency is not shown in Table 3 (column 7), as it could not be identified reliably. Nagarajaiah (2001) has obtained the frequencies and damping ratios of all three modes by using the time domain system identification techniques; the results are shown in Table 3 (columns 8 and 9). The comparison between the computed and identified periods and damping ratios is satisfactory.

IMPACT SPRING AND DASHPOT

An impact-spring stiffness k_g = 5,838 kN/cm (40,000 kip/ft) and impact dashpot c_g = 0 were adopted. Initially an estimated impact dashpot c_g of 108 kN-s/cm (740 kip-s/ft), damping ratio of 17%, was adopted (Nagarajaiah and Sun 1996; Sun 1996). The response reduces for higher values of c_g (Cross and Jones 1993; Nagarajaiah and Sun 1996). However, upon further study c_g was set to zero, as its effect on the impact response due to the earthquake, for 17% damping ratio, was minimal. Also, there was no reliable way of verifying c_g. An estimated gap of 0.305 cm (0.01 ft) was adopted. The reasons for using these values will be explained in the following paragraph. The computed frequencies and damping ratios based on complex eigenvalue analysis for State 2 are shown in Table 4 (columns 4 and 5). Note that in (8) classical eigenvalue analysis results—the frequencies being nearly the same and damping ratios as shown in Table 4—are used. Dynamic analysis with harmonic excitation—of a period equal to the first mode period in State 2—is performed based on (1)–(12) and the response is shown in Figs. 5(a and b). It is clear from the response time histories of the three floors and modes, shown in Figs. 5(a and b), that all three modes are excited during each cycle of impact. The higher modes are damped out before the next cycle of impact.

The aforementioned dynamic analysis computations using an impact-spring stiffness of k_g = 5,838 kN/cm (40,000 kip/ft) and an estimated gap of 0.305 cm (0.01 ft) results in a com-

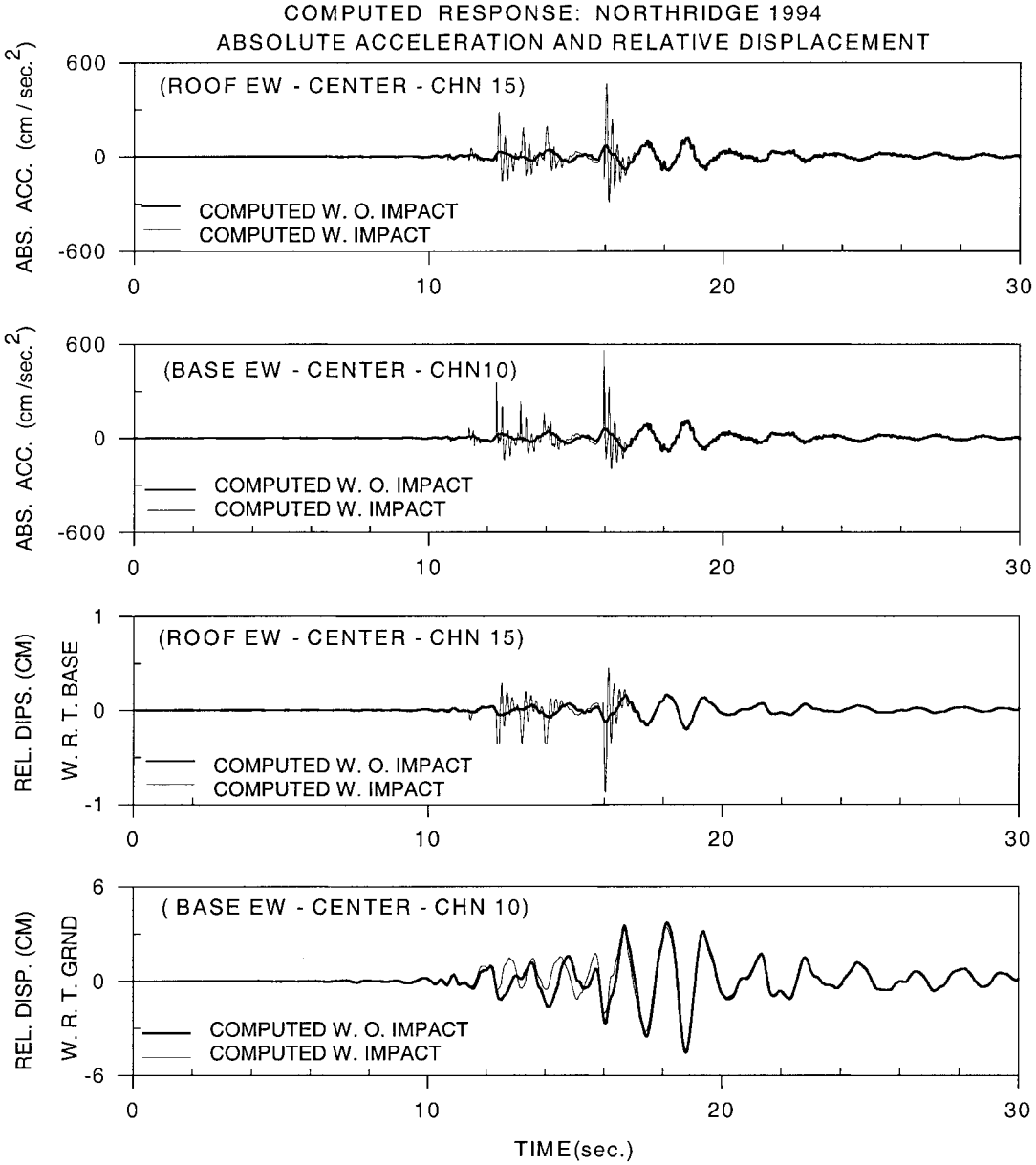

FIG. 8. Computed 2D Response with and without Impact in EW Direction

bined first mode equivalent linear frequency of 1.1 Hz or 0.88 s—an average frequency of the nonlinear combined States 1 and 2—as shown in Table 4 (column 6). Frequency response curves of the combined nonlinear system are shown in Fig. 5(c). The equivalent linear frequency of the combined system is response amplitude dependent. At a harmonic excitation of 0.2 times gravitational acceleration g, the frequency shifts by nearly 1.5—from 0.74 Hz (1.36 s) at $0.02g$ to 1.1 Hz (0.88 s) at $0.2g$. The identified combined first mode period during the time interval 12–16 s shown in Table 4 is 0.84 s in column 7 and 0.94 s in column 8, and the average is 0.88 s, which matches with the computed period. Because the computed and identified periods match for an impact spring stiffness of k_g = 5,838 kN/cm (40,000 kip/ft), it is used in further analysis.

2D RESPONSE IN EW DIRECTION

The 2D response in the EW direction to the Northridge earthquake is computed using the analysis technique described earlier [(1)–(12)] with State 1 and State 2 properties and conditions for state change. A time step of 0.005 s is found to be adequate for obtaining the numerical response. The computed acceleration and displacement response at the base and roof levels are shown in Fig. 6, along with the recorded response. It is evident from the comparison of the recorded and computed response that the analytical model captures the impact phenomenon adequately; it also indicates that the estimated parameters used in the computation are satisfactory.

The estimated gap size variation in the 2D model with one-sided impact at the base level is shown in Fig. 7(a). The impact against the entry bridge occurred between 12 and 16.2 s—after which the entry bridge allowed free motion. The FCC building behaved as a typical base-isolated building after 16.2 s; hence, the time dependent gap $g(t)$ is set equal to the isolation gap after 16.2 s. The computed impact force time history is shown in Fig. 7(b). Also, shown is the estimated impact force time history (Nagarajaiah and Sun 1996; Sun 1996) from the recorded response. The comparison indicates satisfactory agreement.

In Fig. 8 the computed response with and without impact

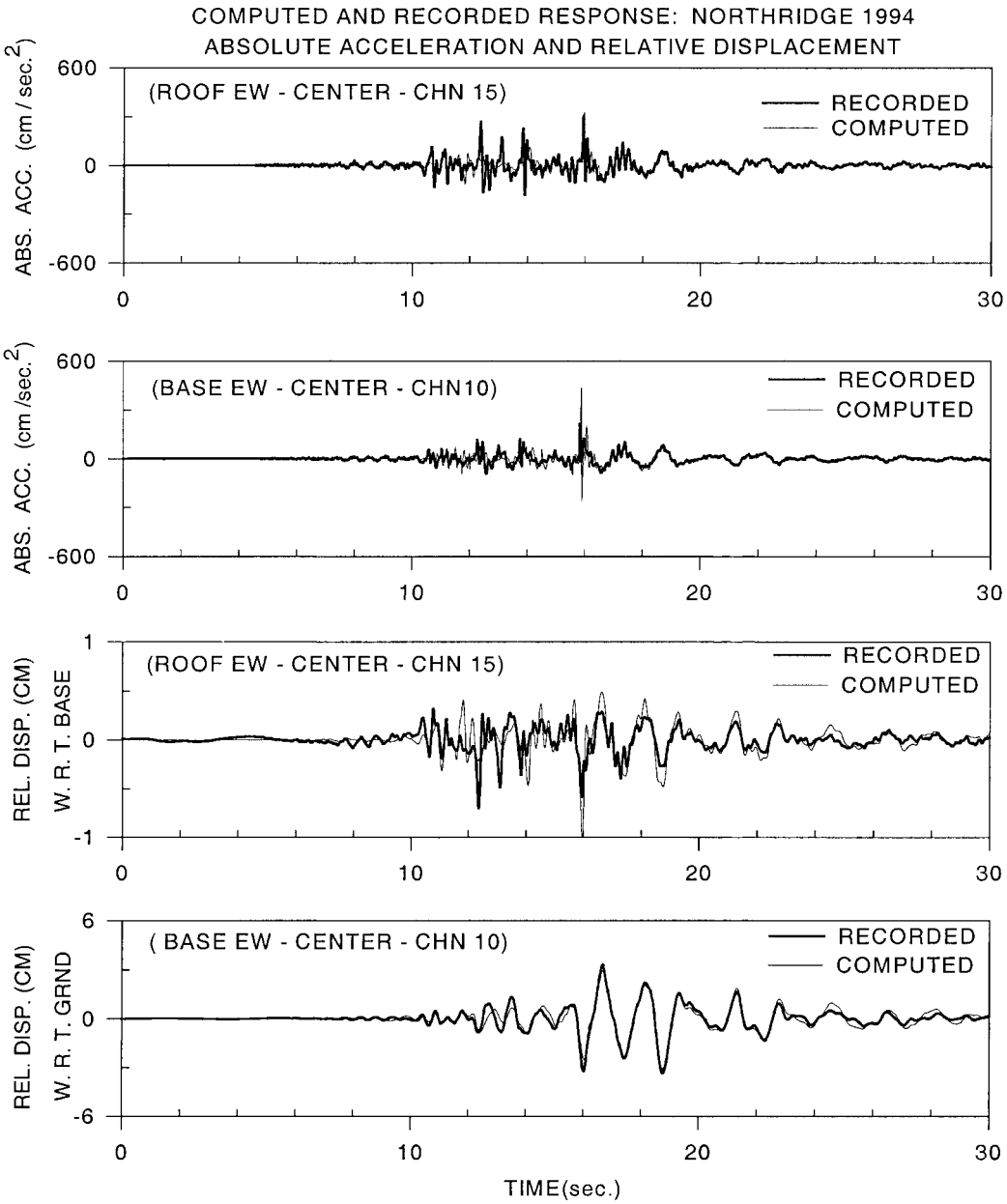

FIG. 9. Comparison of Recorded and Computed 3D Response with Impact

is shown. It is evident from Fig. 8 that impact increases the acceleration and displacement in the superstructure. The response without impact is dominated by first mode response with negligible second and third mode responses. It is evident from the response that the FCC building would have performed well without impact.

3D RESPONSE

For computing the 3D response, the analytical model developed [(13)–(16)] and the impact-spring properties estimated earlier are used; however, the impact spring is located at the northeast corner of the building, as shown in Fig. 1(c). A time step of 0.005 s is found to be adequate for obtaining the numerical response. The computed response is shown in Fig. 9. The agreement between the recorded and computed response with impact is improved further because of the 3D model and the torsional effects being captured appropriately. The torsional effects are absent in the 2D case; hence, the comparison is not as good as the 3D case.

EFFECT OF IMPACT AND EFFECTIVENESS OF BASE ISOLATION

The effects of impact in the EW direction are examined by comparing floor response spectra for (1) the base-isolated building with and without impact; and (2) the fixed-base case without impact, as shown in Figs. 2(d and f). The peak story shears and peak drift envelopes are shown in Fig. 10. It is evident from the results in Figs. 2 and 10 that impact causes (1) an increase in high-frequency/low-period response because of higher mode participation; and (2) an increase in peak story shear and drift. The effectiveness of base isolation is thus reduced. The response of the base-isolated FCC building with impact in the Northridge earthquake is less than the fixed-base case. However, impact should be avoided in base-isolated structures as it can cause increased shear and drift and can cause damage.

There is no indication of impact, in the NS direction, from the time histories shown in Fig. 3(a). The effective isolation period during strong motion, between 15 and 20 s, is nearly 1.4 s, as evident from Fig. 3(a). The isolation system was effective in the NS direction.

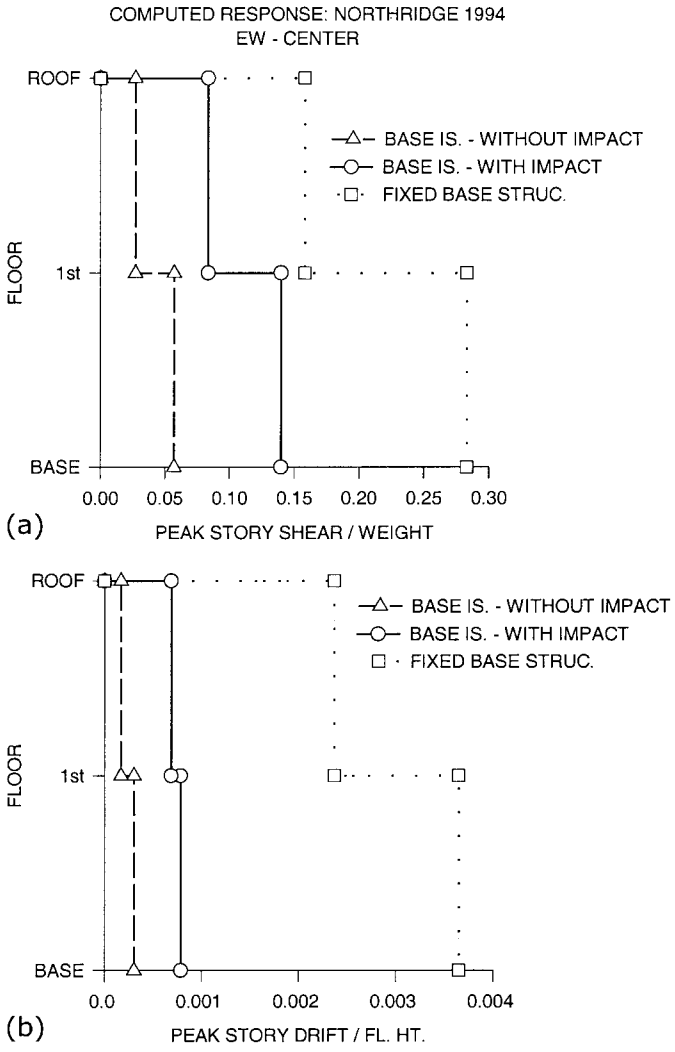

FIG. 10. Comparison between Computed Response of Base-Isolated Structure and Computed Response of Fixed-Base Structure: (a) Normalized Peak Story Shear Envelopes; (b) Normalized Peak Story Drift Envelopes, in EW Direction

DISCUSSION

It is useful to compare this study, completed in 1996 (Nagarajaiah and Sun 1996; Sun 1996) with Malhotra (1997), who studied the dynamics of impacts in base-isolated buildings. He considered uniform shear beam superstructure and perfect isolation (zero stiffness and damping isolation system). He considered the system response in three stages: (1) before impact, the perfectly isolated building, moving as a rigid body with uniform velocity across the height of the building; (2) during impact, the combined isolated building/wall system responding in various modes; and (3) after separation, the perfectly isolated building responding in various modes. He performed a detailed parametric study and showed that the impact duration and base shear can be estimated from the impact velocity and the building fixed-base period. The impact duration computed using his results yielded 0.24 s as compared to the 0.22 s (half the 0.43 s in Table 4, column 4), which is comparable. The base shear/weight computed using his results yielded 0.11 as compared to 0.14 [Fig. 10(a)], a difference of 20%.

CONCLUSIONS

The seismic response and performance evaluation of the base-isolated FCC building including impact has been presented. The comparisons between the computed and recorded responses (verified by system identification) presented indicates that the modeling techniques developed are reliable. Detailed evaluation conducted in the study indicates that impact occurred against the entry bridge in the northeast corner of the FCC building in the EW direction. Impact ceased after a certain duration and the entry bridge allowed free motion of the FCC building to behave as a typical base-isolated structure. Base isolation was effective in the NS direction and reduced the response. It is evident from the evaluation that the base-isolated FCC building performed well, except for impact, which increased structure shear, and drift demands. The effectiveness of base isolation is reduced because of impact. Impact should be avoided in base-isolated structures as it can cause increased shear and drift and can cause damage.

ACKNOWLEDGMENTS

This study was supported by a grant from the CSMIP of the California Department of Conservation (Contract No. 1093-556). The writers are grateful for this support. The writers wish to thank Drs. M. J. Huang, R. G. Darragh, and A. F. Shakal of CSMIP for providing building drawings, bearing test results, and strong motion records.

REFERENCES

Bachman, R. E., Gomez, M. J., and Chang, K. C. (1990). ''Verification

analysis of the base isolated Los Angeles Fire Command and Control Facility.'' *Proc., 4th U.S. Nat. Conf. on Earthquake Engrg.*, 539–548.
Cross, W. B., and Jones, N. P. (1993). ''Seismic performance of joist-pocket connections. I: Modeling.'' *J. Struct. Engrg.*, ASCE, 119(10), 2986–3007.
Earthquake Engineering Research Institute (EERI). (1996). ''Northridge earthquake of January 17, 1994, reconnaissance report.'' *Earthquake Spectra*, 2(January).
Hall, J. F., Heaton, T. H., Halling, M. W., and Wald, D. J. (1995). ''Near-source ground motion and its effects on flexible buildings.'' *Earthquake Spectra*, 11(4), 569–606.
Kelly, J. M. (1993). *Earthquake-resistant design with rubber*, 2nd Ed., Springer, New York.
Ljung, L. (1987). *System identification*, Prentice-Hall, Englewood Cliffs, N.J.
Maison, B. F., and Kasai, K. (1990). ''Analysis for type of structural pounding.'' *J. Struct. Engrg.*, ASCE, 116(4), 957–977.
Malhotra, P. K. (1997). ''Dynamics of seismic impacts in base isolated buildings.'' *Earthquake Engrg. and Struct. Dyn.*, 26, 797–813.
Nagarajaiah, S. (2001). ''System identification of base isolated buildings using 1994 Northridge earthquake response.'' *Struct. Res. at Rice Rep. No. 53*, Rice University, Houston.
Nagarajaiah, S., Reinhorn, A. M., and Constantinou, M. C. (1991a). ''3D-BASIS: Nonlinear dynamic analysis of three-dimensional base isolated structures—Part II.'' *Rep. No. NCEER-91-0005*, Nat. Ctr. for Earthquake Engrg. Res., State University of New York, Buffalo.
Nagarajaiah, S., Reinhorn, A. M., and Constantinou, M. C. (1991b). ''Nonlinear dynamic analysis of 3D-base isolated structures.'' *J. Struct. Engrg.*, ASCE, 117(7), 2035–2054.
Nagarajaiah, S., and Sun, X. (1995). ''Response of base isolated buildings during the 1994 Northridge earthquake.'' *Proc., SMIP95 Seminar*, 41–55.
Nagarajaiah, S., and Sun, X. (1996). ''Response of base isolated buildings in the 1994 Northridge earthquake.'' *Final Rep., Proj. No. 1093-556*, California Strong Motion Instrumentation Program, Sacramento, Calif.
Nagarajaiah, S., and Sun, X. (2000a). ''Response of base isolated buildings during 1994 Northridge earthquake.'' *Struct. Res. at Rice Rep. No. 52*, Rice University, Houston.
Nagarajaiah, S., and Sun, X. (2000b). ''Response of base-isolated USC hospital building in Northridge earthquake.'' *J. Struct. Engrg.*, ASCE, 126(10), 1177–1186.
Nigam, N. C., and Jennings, P. C. (1969). ''Calculation of response spectra from strong-motion earthquake records.'' *Bull. Seismological Soc. of America*, 59(2), 909–922.
Seible, F., and Priestley, M. J. (1989). ''L. A. County Fire Command and Control Center, bearing tests.'' *Rep. No. TR-89/01*, Dept. of Struct. Engrg., University of California, San Diego.
Shakal, A., Huang, M., Darragh, R., et al. (1994). ''CSMIP strong motion records from the Northridge earthquake of 17 January 1994.'' *Rep. No. OSMS. 94-07*, Calif. Strong Motion Instrumentation Program, Division of Mines and Geology, Sacramento, Calif.
Sun, X. (1996). ''Response of base isolated buildings in the 1994 Northridge earthquake.'' MS thesis, University of Missouri, Columbia, Mo.